High-order harmonic generation in rare gases with an intense short-pulse laser

C.-G. Wahlström, J. Larsson, A. Persson, T. Starczewski, and S. Svanberg
Department of Physics, Lund Institute of Technology, S-221 00 Lund, Sweden

P. Salières, Ph. Balcou, and Anne L'Huillier
Service des Photons, Atomes et Molécules, Commissariat à l'Energie Atomique, Bâtiment 522, Centre d'Etudes de Saclay, 91191 Gif-sur-Yvette, France
(Received 17 June 1993)

We present experimental studies of high-order harmonic generation in the rare gases performed with a short-pulse titanium sapphire laser operating at 794 nm in the 10^{14}–10^{15} W/cm^2 range. The harmonic yields generated in neon and in argon are studied for all orders as a function of the laser intensity. They vary first rather steeply, in the cutoff region, then much more slowly in the plateau region, and, finally, they saturate when the medium gets ionized. The dependence of the high-order harmonic cutoff with the laser intensity in neon and argon is found to be lower than that predicted in single-atom theories. We observe high-order harmonics in argon and xenon (up to the 65th and 45th, respectively) at 10^{15} W/cm^2, which we attribute to harmonic generation from ions. We also show how the harmonic and fundamental spectra get blueshifted when the medium becomes ionized.

PACS number(s): 42.65.Ky, 32.80.Rm

I. INTRODUCTION

High-order harmonic generation in gases is one of the most promising ways of producing short-pulse coherent radiation in the soft-x-ray range. The generation of energetic photons by frequency conversion in rare-gas media has now been demonstrated in several laboratories, for example, in Saclay (135th harmonic of a 1053 nm Nd-glass laser [1]), in Stanford (109th harmonic of a 806 nm Ti-sapphire laser [2]), and in Tokyo (25th harmonic of a 248 nm KrF laser [3,4]). Many lasers have been used to produce harmonics, from short-wavelength excimer lasers [3,5,4], visible dye lasers [6,7], to infrared Nd-glass systems [1,8–10]. Among the "state-of-the-art" lasers well adapted for the efficient production of harmonics and their utilization, the titanium sapphire (Ti-S) laser developed recently in Stanford [11] stands out. They have short pulse durations, 100–200 fs, relatively long wavelengths (800 nm), high repetition rates (10 Hz), and broad tunability. The first harmonic generation experiments performed with a Ti-sapphire laser system [2,4,12] have indeed shown that very short wavelengths could be generated in a gas of neon (or helium) atoms, the shortest being about 7 nm, i.e., 170 eV corresponding to the 109th harmonic of 806 nm [2].

In a low-frequency high-intensity regime, the harmonic spectrum presents a characteristic behavior: it falls off for the first few harmonics, then exhibits a *plateau* extending sometimes to more than 150 eV [1,2]. The plateau ends up by a rather sharp *cutoff*. One of the most interesting questions concerns the extension of the plateau. By performing time-dependent calculations for a number of atomic systems in various conditions of laser intensity and frequency, Krause, Schafer, and Kulander [13] predicted that the width of the plateau varies as $I_p + 3U_p$, where I_p is the ionization energy and $U_p = e^2E^2/4m\omega^2$ the ponderomotive energy, i.e., the cycle-averaged oscillation energy of a free electron in the field. e and m are the charge and mass of the electron, E is the field strength, and ω is the laser frequency. The same law can also be found by using simpler models such as the δ-function potential model employed by Becker and co-workers [14,2]. Some insight into the physical meaning of this formula has recently been given by Schafer, Kulander, and Krause [15] and by Corkum [16], using a quasiclassical approach. In this model, electrons first tunnel through the barrier formed by the atomic potential and the laser field [17,18]. Their subsequent motion in the field is treated classically. Only those electrons that return to the nucleus can emit harmonics by recombining to the ground state. The maximum kinetic energy acquired by the electrons from the field when they return to the nucleus is $3.2U_p$, so that the maximum emitted energy is $I_p + 3.2U_p$, close to the prediction of [13]. Thus, harmonic generation in a low-frequency high-intensity regime can be understood as a three-step process: tunnel ionization followed by acceleration of the electron in the field and scattering by the atomic potential leading to recombination back to the ground state.

Recently we have presented [19] an experimental study of the harmonic generation cutoff law using a short-pulse Ti-sapphire laser system. Systematic measurements of the harmonic generation yields in neon have been performed. The experimental cutoff energy was found to be lower than that predicted in single-atom theories [13,14]. To understand this effect, we have investigated the influence of propagation [20,21] and in particular of focusing on the cutoff energy, using single-atom dipole moments obtained from a simple quantum-mechanical theory of harmonic generation valid in the tunneling limit. In a tight focusing limit, i.e., when the length of the medium is larger than the coherence length induced by focusing,

propagation in the nonlinear medium lowers the extension of the harmonic plateau in a significant way, from $I_p + 3.2U_p$ to approximately $I_p + 2U_p$ for the high harmonics.

In the present paper, we give a full account of the experimental part of Ref. [19]. We present systematic experimental studies of harmonic generation not only in neon as described in [19], but also in the other rare gases, in xenon, argon, and helium. The production of the high-order harmonics is investigated over a broad spectral range from 15 to 150 eV (the limits of our spectrometer), in various focusing conditions, and over a broad range of intensities ($10^{14} - 10^{15}$ W/cm^2), both below the saturation due to ionization and above it. We use ionization rates measured in the same experimental chamber, at lower pressure, to check our determination of the focused intensity. The harmonic generation yield is studied for all orders (from the 13th to the 79th in neon and to the 35th in argon) as a function of the laser intensity. The use of a long focal length (2 m) allows us to optimize the number of photons produced in neon and to study the harmonic yields below saturation with a large dynamical range. In xenon and argon at high laser intensity (10^{15} W/cm^2), we see much higher-order harmonics than expected from the cutoff law, which we attribute to harmonic generation in ions. Finally, we show how the harmonic and fundamental spectra get blueshifted (broadened on the blue side) as the medium becomes ionized.

The paper is organized as follows: In Sec. II, we describe the laser system and the experimental apparatus. The main results of this work which consist of systematic studies of intensity dependences in neon and argon are presented in Sec. III and discussed in Sec. IV. Finally, in Sec. V, we present measurements performed above the saturation intensity in xenon and argon. We summarize in Sec. VI.

II. DESCRIPTION OF THE EXPERIMENT

A. Laser system

The laser used in this experiment is the new Ti-sapphire terawatt laser system at the Lund High Power Laser Facility. This system is based on chirped pulse amplification and has unique properties of broad tunability, short-pulse width, high peak power, and high repetition rate (10 Hz). A schematic diagram of the laser is given in Fig. 1.

The oscillator, generating 10 nJ, 100 fs seed pulses, is a Kerr-lens mode-locked Ti-S laser (Coherent Mira) pumped by an argon-ion laser. The seed pulses are stretched to 260 ps in a grating stretcher before being electro-optically injected (at 10 Hz repetition rate) into a regenerative amplifier (RGA). In the RGA, the pulses make 24 passes through a Ti-S crystal pumped by the frequency doubled output from a Nd:YAG laser (where YAG denotes yttrium aluminum garnet). The amplification of the RGA is about 10^6, with output energies of about 10 mJ.

After expanding the beam to a diameter of about 8 mm, the pulses are further amplified in a linear four-pass Ti-S amplifier. This amplifier consists of a single Ti-S crystal, pumped at 10 Hz with up to about 1.4 J of frequency doubled Nd:YAG radiation. The pulse energy after amplification can be varied continuously between about 10 and 450 mJ by varying the amount of pump energy to the final amplifier. Before temporally recompressing the pulses, the beam is further expanded to a diameter of 50 mm. Due to bandwidth narrowing and additional group velocity dispersion picked up during the amplification, the final pulse width after compression is longer than that of the oscillator pulse. The passage through the double-pass grating compressor gives rise to a 40% energy loss. The best characteristics of the final output from this 10 Hz system are 150 fs, 250 mJ, 1.5 TW, a wavelength between 760 and 840 nm, with a 9 nm spectral width at 800 nm. In the experiments described in this paper, the laser was operated at a fixed wavelength, around 794 nm. The peak wavelength of the oscillator was actually set to 792 nm, but in addition to the spectral narrowing in the amplification chain (mainly in the RGA), there is also a slight redshift of about 2 nm. The pulse width, as will be discussed below, was about 250 fs.

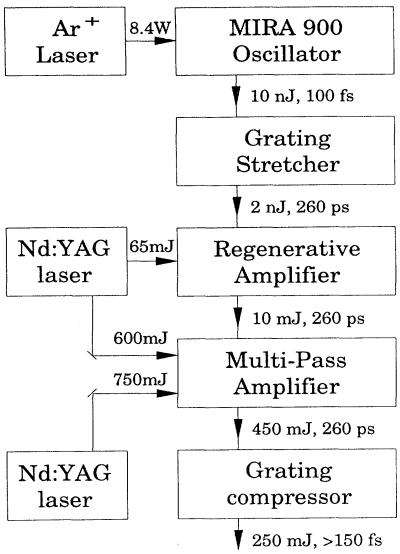

FIG. 1. Schematic diagram of the laser.

B. XUV spectrometer

The spectrometer built up in Saclay for the generation and detection of harmonics is schematically described in Fig. 2. The laser is focused just below the nozzle of a pulsed gas jet by a f=1 m or f=2 m lens. The density of gas in the interaction volume could be varied, but was typically about 20 Torr (7×10^{17} atoms/cm^3). The light is analyzed on axis by a monochromator consisting of a toroidal mirror and a 700 grooves/mm plane grating (Jobin Yvon), both coated with gold. In order to optimize the collection efficiency, we image directly the laser focus, without entrance slit. However, we have added a 1

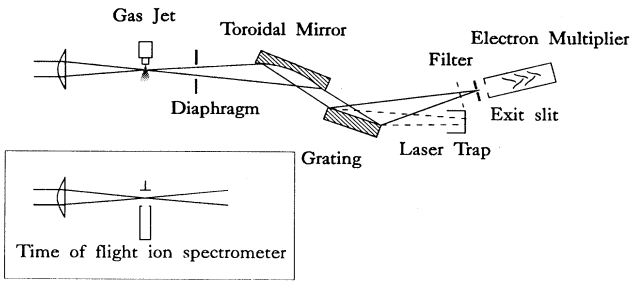

FIG. 2. Experimental setup for the detection of high harmonics. The inset shows the configuration used for the ion measurements.

cm-wide diaphragm at 0.5 m from the focus, in order to reduce the plasma light produced at high laser intensity (in xenon and argon) relative to the harmonic light. The mirror, placed 1 m from the laser focal spot to minimize the risks of damaging the optics with the incident laser light, refocuses the radiation onto a 100 μm output slit. The laser light reflected by the grating is trapped before being focused too much in order to avoid plasma generation on the walls of the chamber. Before the exit slit, we can place free standing aluminium and silver filters, e.g., to eliminate second orders or stray light from the grating. The photons are detected by an electron multiplier. The spectral range covered by this system is approximately 8–80 nm.

One of the most important experimental difficulties is to have a good calibration of the detection system. This requires the knowledge of the spectral efficiencies of the extreme ultraviolet (XUV) optics and of the electron multiplier. We have performed a series of experiments at SuperACO (Super Anneau de Collisions d'Orsay), using the monochromatized synchrotron radiation from the line SA23 (with a spectral range from 20 to 200 eV). In these experiments, the gas jet in Fig. 2 is replaced by an entrance slit, followed by an electron multiplier of the same type as the one placed after the exit slit, which can be moved into and out of the light trajectory. This allowed us to obtain a reliable relative efficiency of our spectrometer from 20 to 160 eV. Unfortunately, we were not able to get an absolute calibration: The number of photons reported in the figures below has been obtained from a previous absolute determination [22] by estimating the absolute gain of the electron multiplier and the optics efficiency. The uncertainty is estimated to about one order of magnitude.

C. Diagnostics and determination of focused intensities

Another experimental difficulty is the determination of the focused laser intensity, which requires the measurement of the laser energy and information on both the spatial and the temporal characteristics of the focused laser pulse.

The incident laser beam has a diameter of approximately 50 mm, but the spatial profile is not Gaussian. In the experiments described in this paper, we always use only the central part of the beam, using hard apertures. We use two different lenses (f=1 m and f=2 m) and apertures of diameters between 17 and 39 mm. Using hard apertures before the focusing lens in a (non-Gaussian) laser beam gives rise to non-Gaussian spatial distributions in the focal plane. These distributions are measured by using microscope objectives placed in the focal region and a charge coupled device (CCD) camera. Thus we obtain, for example, a focal section of 2.6×10^{-5} cm^2, with a 1 m focal lens and a 26 mm iris, i.e., about four times the diffraction limit for a Gaussian beam of diameter 26 mm.

The laser pulse width is determined by autocorrelation techniques. We use a slow scanning autocorrelator with a resolution of about 5 fs. The assumption of a sech^2 temporal profile leads to a full width at half maximum of 250 fs. Below the main narrow peak, we observe a weak shoulder in the autocorrelator trace (about 1 ps long). Using an autocorrelator of second order only, we cannot determine whether this shoulder is due to a slow rise or fall time, or both. However, this broader base contains some fraction of the measured pulse energy and hence influences our intensity determination.

The pulse lengths and spatial profiles are assumed to be constant throughout the experiments. The pulse energies are measured on a shot-to-shot basis using a beam splitter and a calibrated photodiode. The relative intensities are believed to be accurate to within 5%. However, due to the reasons described above, the absolute intensity must be assigned an uncertainty of about $\pm$ 50%.

The absolute intensity can also be inferred by performing ions measurements in the same experimental conditions. The pulsed gas nozzle is removed (see the inset in Fig. 2) and the vacuum chamber is filled up with a static gas pressure below 10^{-6} Torr. The ions produced by the focused laser radiation are collected by a simple 20-cm-long time-of-flight spectrometer. Some of the results obtained in argon, neon, and xenon are shown in Fig. 3. In this figure we also indicate theoretical ionization curves, obtained using the tunneling ionization

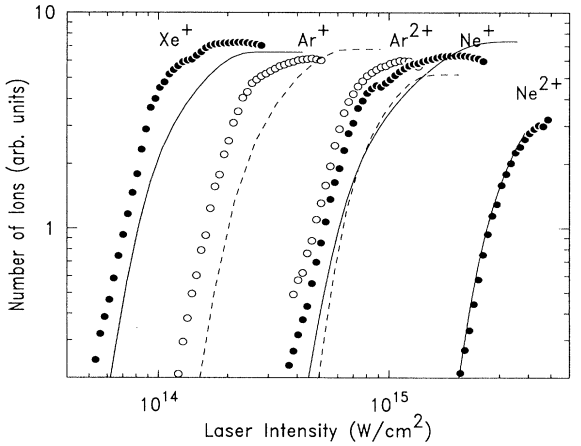

FIG. 3. Xe^+ (full circles), Ar^+, Ar^{2+} (open circles), Ne^+, and Ne^{2+} (full circles) ions as a function of the laser intensity. The lines (dashed for the Ar ions and solid for the Xe and Ne ions) are the predictions from tunnel ionization.

formula of Ammosov, Delone, and Kraïnov [18,23]. Due to the long focal length used and the small acceptance angle of the time-of-flight spectrometer (limited by a 5 mm pinhole at about 1.5 cm from the focus) we do not collect all of the ions produced (in particular the singly charged ions), so that the relative number of ions of different charges produced has no physical significance. This also explains why the dynamical range in these experiments is not more than about two orders of magnitude. We obtain an excellent agreement between the experimental results and the theoretical predictions if we shift our intensity by a factor of 25%. This shift is well within our experimental error bar on the determination of the focused intensity.

III. EXPERIMENTAL RESULTS

A. Harmonic spectra

In Fig. 4, we show typical spectra obtained in xenon, argon, and helium with the 1 m lens. These spectra are obtained by moving the grating in steps of 0.5 Å and by averaging the signal over 30 shots, only accepting pulses within a narrow energy window. The instrumental resolution is approximately 0.5 Å. In contrast with previous measurements performed with longer-pulse lasers [1], the spectral width of the lowest-order harmonic peaks exceeds the resolution of the monochromator, which explains why the width decreases with the harmonic order in Fig. 4. However, due to the absence of an entrance slit, the recorded width is a complex function of the harmonic spectral width.

The spectra in Xe and Ar have been obtained at very high laser intensity, about 10^{15} W/cm^2, much above the saturation intensities for these gases (see Fig. 3). The decrease in the harmonic distribution is not very sharp: The intensity of the harmonics starts decreasing from the 15th harmonic in xenon and from the 21st in argon, but very slowly and it extends very far out, up to the 39th harmonic in xenon in this spectrum (up to the 45th harmonic at a higher intensity) and up to the 65th harmonic in argon. We will come back to the interpretation of these higher-order harmonics in Sec. V A. The signal-to-noise ratio is extremely high for the lowest-order harmonics (10^3 in argon, 10^4 in xenon). The background noise observed in the region below 40 nm in Xe and 25 nm in argon is due to stray light from the grating arising from the very intense low-order harmonics. The use of aluminium filters reduces this noise, which comes from lower-energy ultraviolet light.

The spectrum recorded in helium extends to much shorter wavelengths, down to about 8 nm. In this case, the decrease observed from the 81st harmonic is the cutoff of our spectrometer [1]. Below 10 nm, both the response of the grating and the reflectivity of gold with which the optics are coated, decrease quite rapidly, thus inducing a rather sharp instrumental cutoff [see Fig. 4 (c)]. The background is due to overlap of the harmonic peaks in this spectral region.

B. Study of the extension of the plateau as a function of intensity

In Fig. 5, we show the number of photons in argon (a) and in neon (b) as a function of the harmonic order for several intensities (see the figure caption). The number

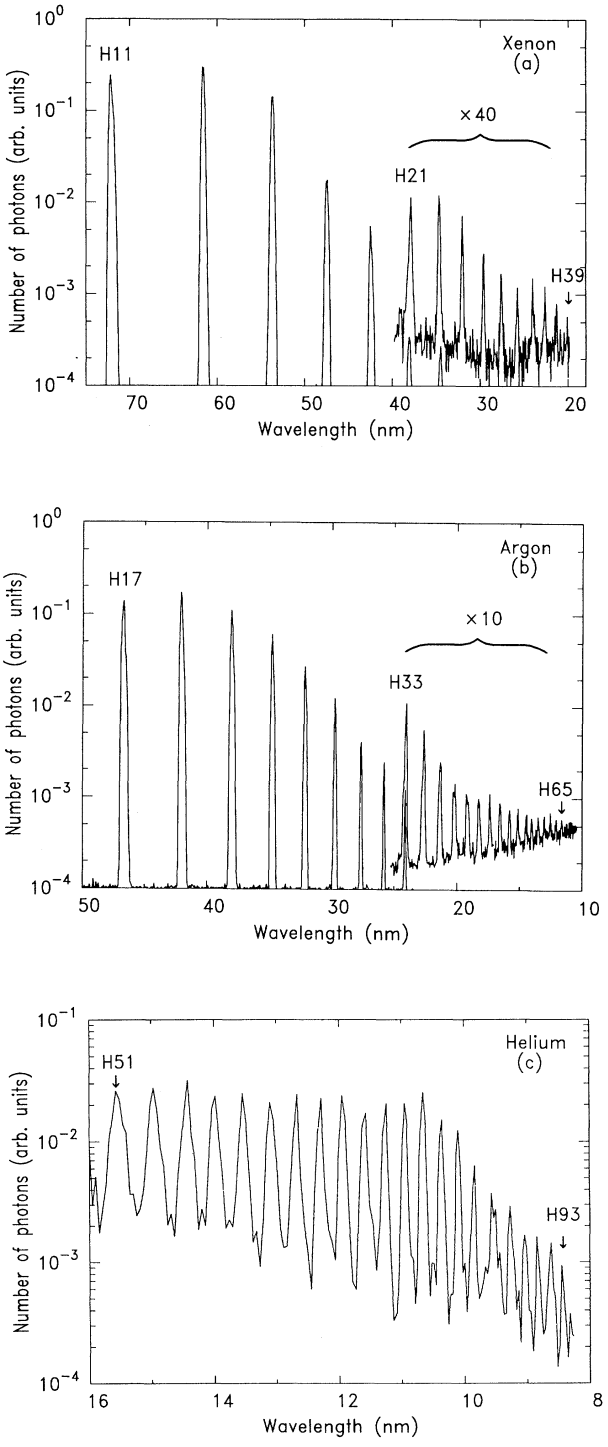

FIG. 4. Harmonic spectra in (a) Xe, (b) Ar, and (c) He. The laser intensity is approximately 10^{15} W/cm^2.

of photons is calculated by taking into account the spectral response of the monochromator, assuming a constant width (equal to the instrumental width of 0.5 Å) for all orders. This leads to an overestimation of the high-order harmonics relative to the (broader) low-order ones. The error, however, is estimated to be less than a factor of 3.

The spectra exhibit the characteristic plateau and cutoff features, apart from the neon spectrum obtained at the highest intensity. The latter shows no cutoff, because of the limitation of our spectrometer towards short wavelengths. As the intensity increases, the strength of the harmonics in the plateau slowly increases and more harmonics join the plateau. This is true up to the saturation intensity, at which the medium ionizes. This intensity is estimated to be about 2.5×10^{14} W/cm^2 in argon and 8×10^{14} W/cm^2 in neon (see Fig. 3). The spectra at the highest intensity in Figs. 5(a) and 5(b) have been obtained just above the saturation intensity for the two gases.

The ionization cross section of argon exhibits a Cooper minimum at about 48 eV [24,25]. The harmonic strength is proportional to the probability for the electron to recombine to the ground state and therefore to the field-free ionization cross section [15,16,19]. The harmonic spectra obtained with a Nd-glass laser system [1] and with a shorter pulse (120 fs) Ti-sapphire laser [26] indeed show a minimum at the 41st harmonic of the Nd-glass system ($\omega = 1.17$ eV) and at the 31st harmonic of the Ti-S laser ($\omega = 1.54$ eV). The spectrum obtained at the highest intensity in Fig. 5(a) shows a structure around the 29th–31st harmonic, whic we believe to be a trace of this Cooper minimum. Unfortunately, in our experimental conditions, the medium ionizes before the harmonics in the Cooper minimum region reach the plateau.

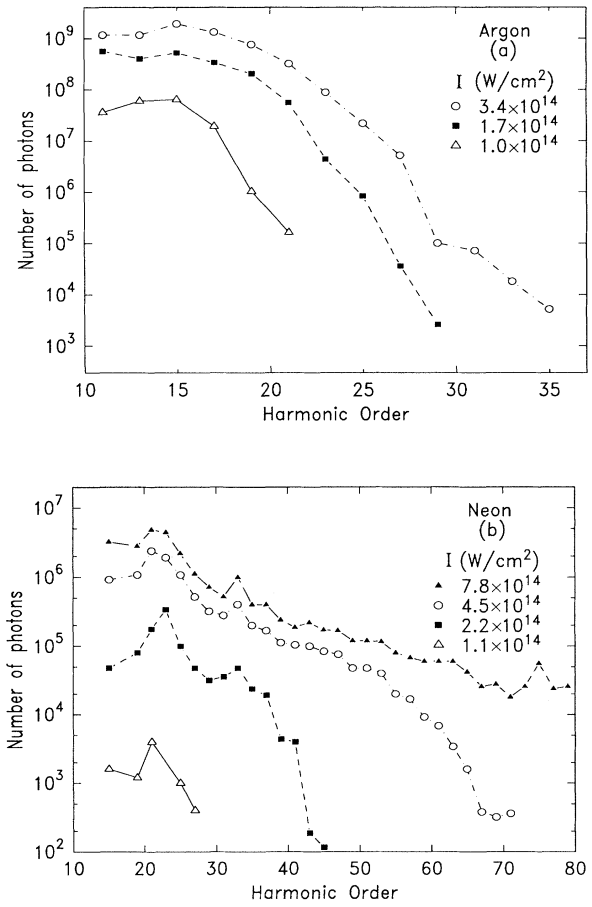

FIG. 5. Number of photons as a function of the harmonic order: (a) argon, the intensities are 3.4×10^{14} W/cm^2 (open circles), 1.7×10^{14} W/cm^2 (full squares), and 10^{14} W/cm^2 (open triangles); (b) neon, the intensities are 7.8×10^{14} W/cm^2 (full triangles), 4.5×10^{14} W/cm^2 (open circles), 2.2×10^{14} W/cm^2 (full squares), and 1.1×10^{14} W/cm^2 (open triangles).

The precise determination of the cutoff energy in these spectra is not easy, because the cutoff is not sharp, especially at high laser intensity. We have used another method, based on the study of the harmonic yields as a function of the laser intensity [2]. The harmonic strength varies much more rapidly with the laser intensity in the cutoff region than in the plateau. It exhibits a marked change of slope (in a logarithmic scale) as it goes from the cutoff to the plateau. This is illustrated in Fig. 6, showing the variation with intensity of the 15th harmonic in argon. Each data point corresponding to one energy bin represents an average of over 100 shots. The circle indicates the intensity at which the 15th harmonic joins the plateau. The curve saturates at higher laser intensity (above 2×10^{14} W/cm^2), when the medium ionizes (see Fig. 3).

In Fig. 7(a)–7(e), we plot the harmonics obtained in neon from the 19th to the 79th. The use of a very long focal length (2 m) allows us to have a good dynamical range of almost four orders of magnitude. The harmonics appear successively as the intensity increases. This is not true for the low-order ones, from the 13th to the 19th, which appear at approximately the same laser intensity (10^{14} W/cm^2). The harmonic strength varies first rather rapidly with the laser intensity in the cutoff region.

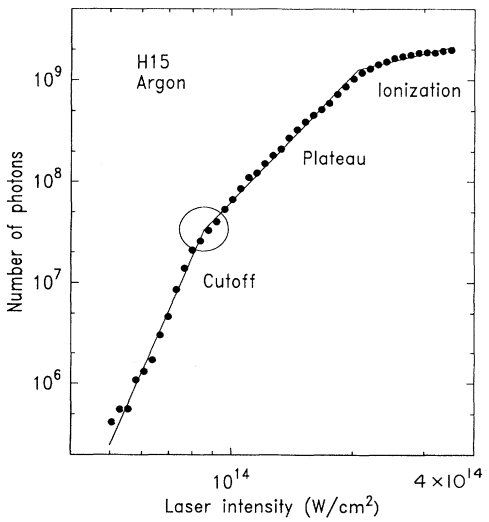

FIG. 6. Number of photons at the 15th harmonic in argon as a function of the laser intensity.

Then they reach the plateau and exhibit a much slower dependence with the laser intensity. As the harmonic order increases, the variation in the cutoff region becomes more rapid and the variation in the plateau slower. For example, the 35th harmonic varies approximately as I^{16} in the cutoff region and as I^3 in the plateau.

In Fig. 8, we plot the harmonics obtained in argon from the 19th to the 35th. The intensity dependences are similar to those obtained in neon for the lowest-order harmonics. Note the drop of the numbers of photons at the 29th and 31st harmonics, corresponding to the position of the Cooper minimum (see the above discussion). The highest-order harmonics (31st, 33rd, and 35th) appear at a higher laser intensity, above saturation (2.5×10^{14}

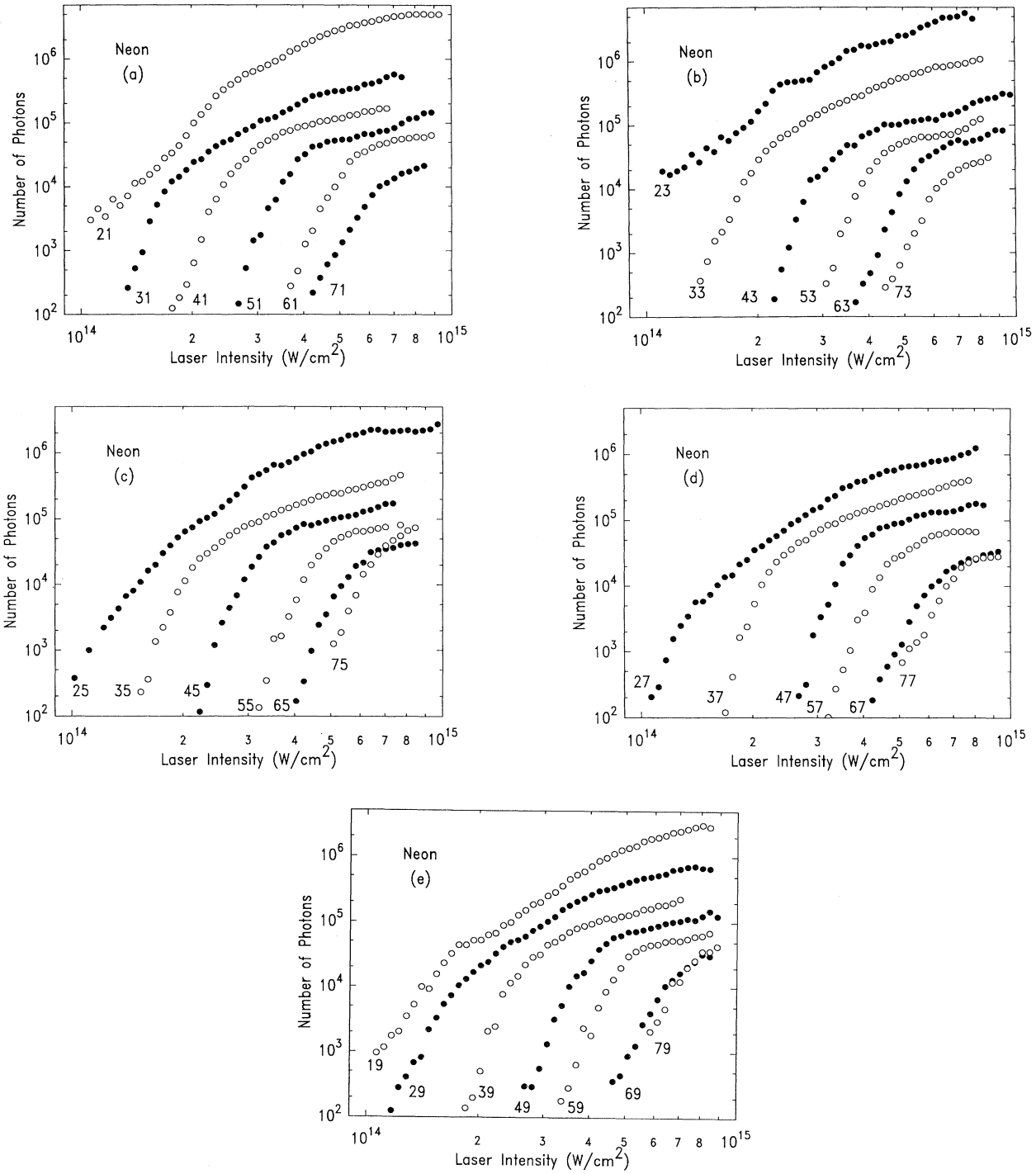

FIG. 7. Number of photons in neon as a function of the laser intensity: (a) harmonics 21,31,41,51,61,71; (b) harmonics 23,33,43,53,63,73; (c) harmonics 25,35,45,55,65,75; (d) harmonics 27,37,47,57,67,77; (e) harmonics 19,29,39,49,59,69,79.

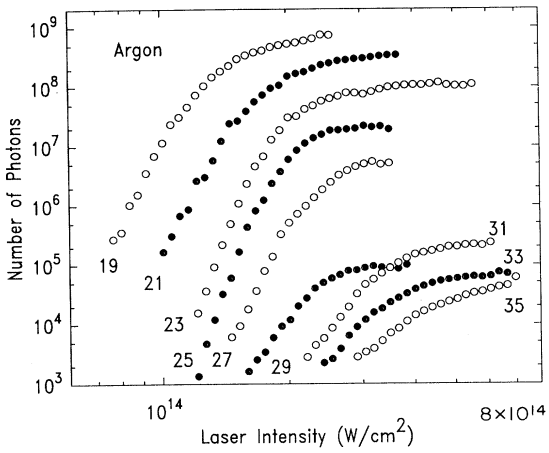

FIG. 8. Number of photons in argon as a function of the laser intensity from the 19th to the 35th harmonic.

W/cm^2). They vary quite slowly with the laser intensity.

In Fig. 9, we compare the intensity dependences of the 15th harmonic in xenon, argon, and neon. We have adjusted the horizontal and vertical scales to make the three curves coincide at low intensity. The intensity dependences are very similar for the three gases. The main difference is the position of the saturation intensity, relative to the intensity at which the harmonic joins the plateau. In xenon, the medium ionizes before the 15th harmonic reaches the plateau. In argon, there is approximately a factor of 2.5 between the two intensities. Finally, in neon, the saturation intensity is barely reached and the plateau grows over almost one order of magnitude in intensity. Below saturation, the three curves are remarkably similar, which seems to point out to a weak atomic dependence in this low-frequency high-intensity regime.

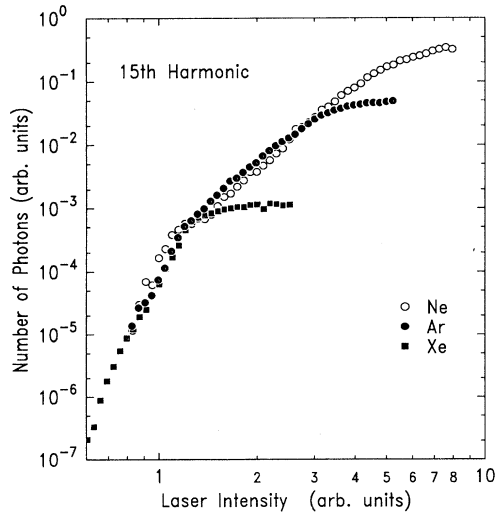

FIG. 9. Comparison of the intensity dependences of the 15th harmonic in Xe (full squares), Ar (full circles), and Ne (open circles).

IV. STUDY OF THE CUTOFF LAW

A. Results in neon

In Fig. 10, we report the position of the change of slope observed in the intensity dependences (see Fig. 7) for all of the harmonics in neon from the 13th to the 79th. We express the intensity in units of the ponderomotive energy $U_p = 5.9 \times 10^{-14} I$ (with I, the laser intensity, in W/cm^2). The vertical scale on the right is the harmonic order, the one on the left is the harmonic photon energy. There are two ways to read this plot: It gives the position of the cutoff intensity for a given harmonic, i.e., the intensity at which the harmonic reaches the plateau. It also gives the maximum energy of the plateau (cutoff energy) for a given intensity. The first conclusion is that the points corresponding to the harmonics higher than the 27th are aligned. A linear regression gives a cutoff law equal to $21 + 2.4U_p$. For comparison, we show the single-atom prediction $21.6 + 3.2U_p$ in dashed line. The cutoff law determined experimentally is significantly lower than that predicted by the single-atom results. If we use the intensity determination obtained by comparing our ion measurements to tunnel ionization predictions, the experimental intensity is increased by a factor of 25%, which gives an even lower cutoff law, equal to $21 + 1.9U_p$. Although our experimental uncertainty on the laser intensity does not allow us to say unambiguously that the measured cutoff is lower than the single-atom prediction, there is a strong indication, based on the ion measurements, that it is indeed the case.

B. Results in argon

We have performed the same analysis in argon and the results are shown in Fig. 11. The cutoff energy for the argon harmonics below the 29th varies as $10 + 2.4U_p$. The ionization energy in argon is equal to 15.8 eV. Again,

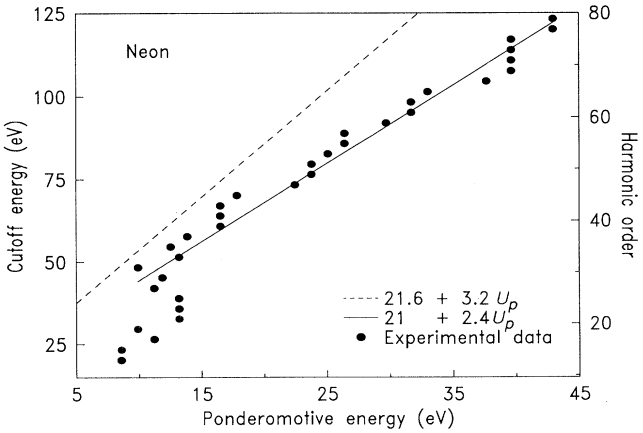

FIG. 10. Cutoff energy in neon as a function of the ponderomotive energy. The solid line is a linear best fit: $21 + 2.4U_p$, the dashed line is the prediction of the single-atom response $21.6 + 3.2U_p$.

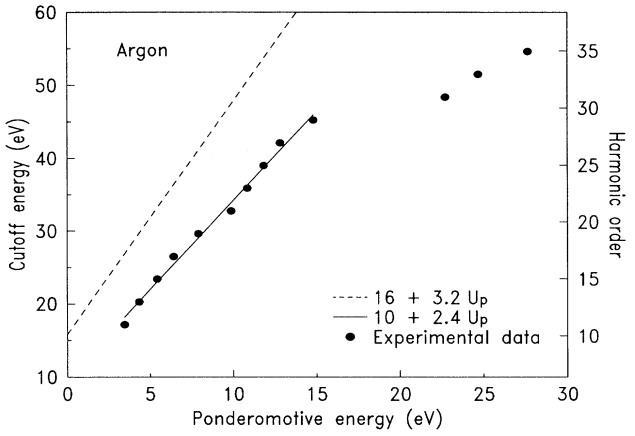

FIG. 11. Cutoff energy in argon as a function of the ponderomotive energy. The solid line is a linear best fit: $10 + 2.4U_p$, the dashed line is the prediction of the single-atom response $16 + 3.2U_p$.

these experimental results indicate that the measured cutoff law is lower than the one predicted in the single-atom response (shown in dashed line). The reason why the coordinate at the origin seems to be lower than the expected 16 eV is not clear at present. It could simply be due to the experimental inaccuracy. The cutoff energy saturates for the harmonics beyond the 29th simply because the medium becomes ionized before these high harmonics reach the plateau. The saturation intensity is equal to 2.5×10^{14} W/cm^2, which corresponds to a ponderomotive energy of 15 eV from which the points deviate from the $10 + 2.4U_p$ line.

C. Discussion

A possible origin for this lower cutoff is the effect of propagation in a tight focusing geometry. In Ref. [19], we examine in detail phase-matching effects in this low-frequency high-intensity regime. We have performed series of calculations in various geometries in order to illustrate the difference between a loose and a tight geometry for the intensity dependence of the cutoff energy. We refer the reader to [19] for more details about the calculations and the comparison between theory and experiment. Briefly, the physical idea is the following. In a tight focusing geometry, phase matching depends strongly on the variation of the polarization with intensity [21]. When this variation is rapid, as is the case in the cutoff region, the polarization is mostly concentrated close to the focus, with maximum cancellation effects between the fields created before and after the focus, and consequently, poor phase matching. When the variation of the polarization with intensity is slow, the volume of emitting dipoles is more important, the near-field profile gets distorted, the cancellation effects are reduced, and phase matching is much more efficient.

Consider how a given harmonic varies with the laser intensity, in the single-atom response and in the many-atom response. There are three intensity regions.

(i) The peak intensity is lower than the intensity at which the harmonic reaches the plateau in the single-atom response. Then, the microscopic harmonic emission varies rapidly with the laser intensity. Phase matching is poor, but stays approximately constant. The variation with intensity of the macroscopic emission follows that of the single-atom response.

(ii) The peak intensity is higher than that needed for the harmonic (emitted by a single atom) to be in the plateau, but there is a significant part of the interaction volume that experiences a lower intensity, corresponding to the cutoff region for the single-atom response. In this intensity region, the microscopic emission rate varies more slowly and exhibits oscillations [2,19,27]. In contrast, phase matching increases rapidly, because the volume contributing to the emission increases.

(iii) The peak intensity is such that most of the volume experiences an intensity corresponding to the plateau region for the single-atom response. Both the microscopic emission and the contribution of phase matching vary slowly with the laser intensity.

Consequently, if the geometry is of the tight focusing type, the change of slope in the intensity dependence of the harmonic strength will occur at a higher intensity in the many-atom response than in the single-atom response, when both the single-atom emission rate and the contribution of phase matching vary slowly with intensity. In other words, at a given intensity, the cutoff energy will be lower in the many-atom response than in the single-atom response.

Focusing becomes a limitation to harmonic generation when the geometrical coherence length ($L_{\rm coh}$) is comparable or smaller than the length of medium L. The coherence length for qth-order harmonic generation can be approximated by the simple expression $L_{\rm coh} = \pi b/2(q-1)$, where b is the laser confocal parameter. Calculations performed in Ref. [19] in neon for our experimental conditions (i.e., a confocal parameter b estimated to 1.3 cm and an interaction length L of 1 mm) show that the cutoff energy shifts from $I_p + 3.2U_p$ to about $I_p + 2U_p$ when $L_{\rm coh}$ becomes smaller than $0.7L$, i.e., from the 29th harmonic. The results of these calculations are consistent with our experimental data, especially when using the intensity determined from the ion measurements. They explain the lower cutoff for the high harmonics such that the geometry is of the tight focusing type and also the higher slope observed for the lower-order harmonics (generated in a loose geometry).

The results obtained in argon (see Fig. 11) are more difficult to explain, since the lower cutoff is observed for the lowest orders, such that the beam is rather loosely focused. The change of geometry coincides with the ionization of the medium. We think that a better understanding of these results could only be achieved by performing more complete calculations on this particular atomic system. The existence of the Cooper minimum makes the determination of the cutoff energy more difficult, at least for a certain range of intensities.

V. HARMONIC GENERATION IN AN IONIZED MEDIUM

Finally, we have studied the generation of harmonics in xenon and argon at very high intensity, such that the

medium is significantly ionized. Our aim was twofold: to observe harmonic generation from ions and to measure the deformation of the spectral profile (blueshift) of the fundamental and of the harmonics in parallel as a function of intensity and gas pressure.

A. Harmonic generation from ions

In Fig. 12, we show spectra obtained in Xe (open circles) and Ar (full circles) at about 10^{15} W/cm^2, using the 1 m lens. The figure uses several sets of data taken in the same conditions, including in particular those shown in Figs. 4(a) and 4(b), which explains why there are sometimes two points corresponding to the same harmonic. The open triangles correspond to data points in xenon obtained at a slightly higher laser intensity (estimated to 2×10^{15} W/cm^2).

The positions of $I_p + 3.2U_p$ at the saturation intensities determined experimentally for the two rare gases (see Fig. 3) are indicated in the figure. The second plateaus observed both in xenon and in argon up to the 45th and to the 65th harmonics, respectively, extend far beyond the cutoff expected for the harmonic emission from a single neutral atom (and *a fortiori* for the emission from the neutral medium). The intensity is higher than the saturation intensity for Xe^+ and Ar^+ ions (see Fig. 3) and therefore high enough for the generation of harmonics from these ions. Note that the levels of the two plateaus differ by almost five orders of magnitude. This comes from the reduced efficiency in the single-ion response [13,28] and from the poorer phase matching in ionized media, influenced by the free electron dispersion.

We have not studied this harmonic emission in more details, because of the low signal-to-noise ratio [see Fig. 4(a) and 4(b)]. These high-order harmonics could only be observed in a certain window of intensity and gas pressure (20 Torr). Varying the intensity, density, focus position, etc. leads to a decrease in the signal-to-noise ratio and the disappearance of those high-order harmonics. This is also why no second cutoff was detected. However, we think that the existence of these harmonics at a fairly high intensity can only be understood by invoking the contribution of ions (and possibly of multiply charged ions in the xenon case). Although harmonic generation from ions has been observed previously using high-frequency lasers (KrF) [3–5,13,28], this paper presents evidence for emission from ions with a low-frequency laser, with possibilities of producing much higher photon energies.

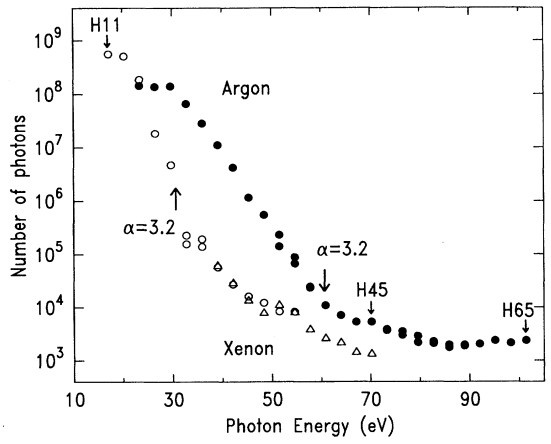

FIG. 12. Harmonic spectra in Xe (open symbols) and in Ar (full circles) at about 10^{15} W/cm^2. The position of the single-atom cutoff energy at the saturation intensities for the two rare gases is indicated by the arrow with the label $\alpha = 3.2$.

B. Blueshift of the fundamental

The shift towards shorter wavelengths of a short-pulse laser focused into a gaseous medium has been observed previously in a cell geometry (at a much higher pressure) [29] and also in a gas jet, in a very similar configuration [2]. It has been discussed in several theoretical papers [21,30]. The blueshift originates from the free electrons created during the laser pulse, which induce a variation of the refractive index [21],

$$\delta n_1(\mathbf{r}, z, t) = -\frac{2\pi e^2}{m\omega^2}\mathcal{N}_e(\mathbf{r}, z, t), \tag{1}$$

where ω denotes the laser frequency and $\mathcal{N}_e(\mathbf{r}, z, t)$ the electron density. The time variation of the index (i.e. of the phase) leads to a spectral blueshift of the fundamental field. The space variation of the index leads to defocusing of the beam [31,30], so that the peak intensity in vacuum is never reached in a dense medium. The precise calculation of the blueshift at a given intensity requires us to perform a complete propagation calculation including not only the phase modulation induced by ionization but also these refraction effects which reduce the effective intensity in the medium. However, the expected blueshift can be estimated simply by the following expression (CGS units),

$$\delta\lambda_1 = -\frac{\lambda^3 e^2}{2\pi m c^3}\frac{d\mathcal{N}_e}{dt}L. \tag{2}$$

At saturation, we can approximate $d\mathcal{N}_e/dt$ by $\mathcal{N}_0/\tau$, where $\mathcal{N}_0$ is the initial atomic density and τ is the laser pulse width. In our experimental conditions (20 Torr, λ = 794 nm, L = 1 mm), the expected blueshift is 2 nm.

In the experiment, the spectrum of the fundamental is recorded after the interaction with the nonlinear medium, by using some of the light scattered in the chamber, further guided through an optical fiber and lens coupled to an f=27 cm Acton spectrometer. The output of the spectrometer is imaged onto an optical multichannel analyzer and detected by a gated, image intensified, 1024 channel diode array. In Fig. 13, we show the spectra of the fundamental (integrated over 200 laser shots) at three different laser intensities, 6.5×10^{13} W/cm^2, 1.1×10^{14} W/cm^2 (just above the saturation intensity of xenon), and 2.3×10^{14} W/cm^2. The pressure in the xenon gas jet is 20 Torr. The spectrum taken at the lowest intensity is similar to the spectra taken without gas, even at high intensity. The observed structures are reproducible and exist without gas. The spectra exhibit a net shift

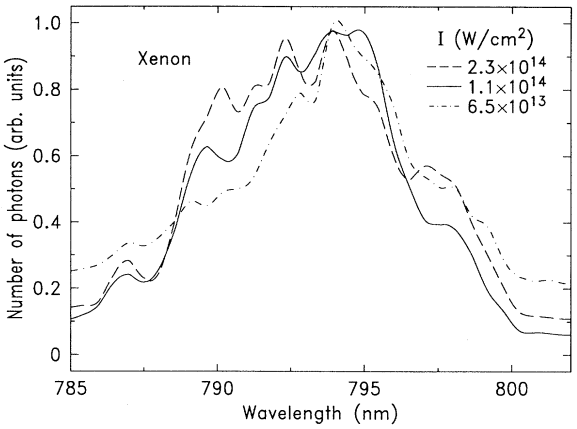

FIG. 13. Normalized spectra of the fundamental beam after interacting with a 20 Torr gas jet of xenon. The intensities are 6.5×10^{13} W/cm^2 (dot-dashed line), 1.1×10^{14} W/cm^2 (solid line), and 2.3×10^{14} W/cm^2 (dashed line) .

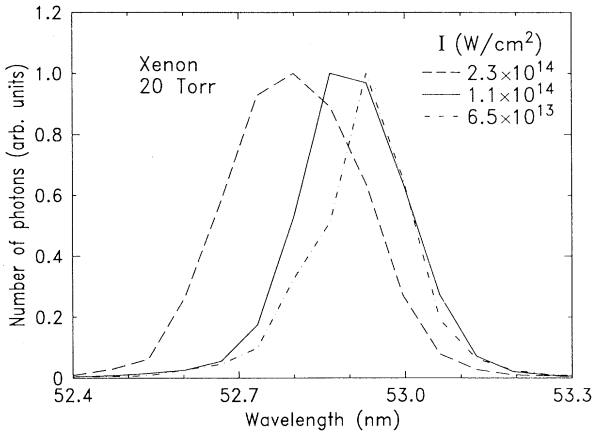

FIG. 14. Normalized spectral profiles of the 15th harmonic in xenon at 20 Torr. The intensities are 6.5×10^{13} W/cm^2 (dot-dashed line), 1.1×10^{14} W/cm^2 (solid line), and 2.3×10^{14} W/cm^2 (dashed line).

towards short wavelengths, equal to 2 nm for the highest intensity one, in good agreement with the previous estimation. This value is also very close to the result obtained by Macklin, Kmetec, and Gordon [2] in neon instead of xenon, but otherwise similar conditions.

C. Blueshift of the harmonics

The spectral shift of the harmonics originates from the variation of the refractive index at frequency $q\omega$ and from the spectral shift of the fundamental. The latter is simply $\delta\lambda_q = \delta\lambda_1/q$ ($\delta\omega_q = q\delta\omega_1$), whereas the shift induced by the propagation of the harmonics in the medium [see Eqs.(1) and (2)] is $\delta\lambda_q = \delta\lambda_1/q^3$ ($\delta\omega_q = \delta\omega_1/q$) [21,32]. The effect of the free electrons is much smaller than the effect of the shift of the fundamental field for the high harmonics and one expects the shift of the harmonics to be equal to the ratio of the fundamental shift by the process order.

Our XUV spectrometer, with no entrance slit and a 100 μm output slit, does not allow us to measure the true spectral distribution of the individual harmonics. However, thanks to the short-laser-pulse duration, the linewidth of the lower-order harmonics becomes noticeably greater than the experimental width imposed by the XUV spectrometer (0.5 Å). We can therefore study the variation of the spectral width and shift of these harmonics with the laser intensity or gas pressure and we can correlate the shift of the harmonics to that of the fundamental.

In Fig. 14, we show the spectral profiles of the 15th harmonic in xenon obtained at the same intensities and pressure as in Fig. 13. At the lowest intensity, the harmonic width at half maximum is 1.7 Å. As the intensity is increased, the profile broadens significantly (2.3 Å at 1.1×10^{14} W/cm^2, 3 Å at 2.3×10^{14} W/cm^2) and the central wavelength shifts. The blueshift of 1.5 Å between the spectral profiles from the lowest to the highest intensity is consistent with the one observed on the fundamental. Note that the harmonic profile at highest intensity is not broad enough to include the original unshifted wavelength.

The spectral width of the harmonics can be estimated by the difference between the measured value and the 0.5 Å spectral resolution of the instrument. This gives spectral widths varying from 1.2 Å at the lowest intensity to 2.5 Å at the highest. By comparison, lowest-order perturbation theory predicts a width of about 1.7 Å for the 15th harmonic (for a 9 nm fundamental width).

In Fig. 15, we compare the spectral profiles of the 15th harmonic in xenon, at the same laser intensity (1.1×10^{14} W/cm^2) at three pressures, 20 Torr, 30 Torr, and 40 Torr. The width of the harmonic is almost constant. The increase of gas pressure alone induces no additionnal spectral broadening, only a global displacement of the profile. The blueshift depends linearly on the initial atomic density, which is exactly verified from this result.

Finally, we present in Fig. 16 the spectral profiles of

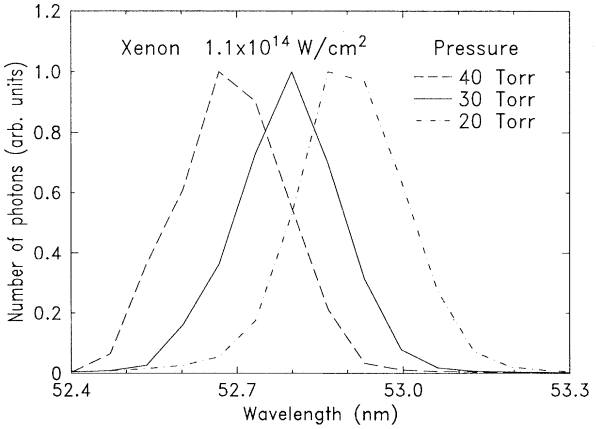

FIG. 15. Normalized spectral profiles of the 15th harmonic in xenon at 20 Torr (dot-dashed line), 30 Torr (solid line), and 40 Torr (dashed line). The intensity is 1.1×10^{14} W/cm^2.

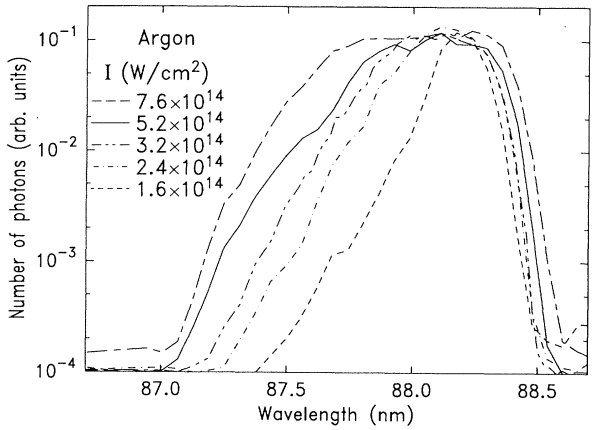

FIG. 16. Normalized spectral profiles of the 9th harmonic in argon at 20 Torr. The intensities are 1.6×10^{14} W/cm^2 (dashed line), 2.4×10^{14} W/cm^2 (dot-dashed line), 3.2×10^{14} W/cm^2 (double-dot-dashed line), 5.2×10^{14} W/cm^2 (solid line), and 7.6×10^{14} W/cm^2 (long-dash–short-dashed line).

the 9th harmonic in argon at several intensities (see figure caption) and at a 20 Torr pressure. The spectral profile broadens to the blue side of the spectrum and its central wavelength shifts to shorter wavelengths as the intensity increases. The shift of the blue side is still consistent with what can be inferred from the blueshift measurements of the fundamental beam. In contrast to the 15th harmonic in Xe, the profile always extends to the unshifted wavelength on the red side.

Both spatial and temporal effects [33] can affect significantly the shift and broadening of the spectral line shape as a function of the laser intensity. In the spatial domain, the amount of blueshift is more important on axis, where the intensity varies more rapidly, than away from it. In the time domain, the amount of blueshift depends on whether or not the harmonic is predominantly created at the beginning of the laser pulse (with little ionization and consequently a small spectral distortion of the fundamental) or later in the pulse. This leads to a complex intensity-dependent spectral shift and broadening of the harmonic line shape, strongly dependent on the variation with intensity of the nonlinear polarization, in the region of the saturation intensity. In particular, the spectral distortion of the harmonics should depend on whether the harmonic has reached the plateau regime at saturation. This could explain the difference between the results shown in Fig. 14 and in Fig. 16. As shown in Fig. 9, the 15th harmonic in xenon belongs to the cutoff region up to the saturation intensity whereas there is a large intensity range before saturation where the 9th harmonic in argon belongs to the plateau regime, with a slow intensity dependence. Consider the generation of the 9th harmonic at a peak intensity above saturation. The harmonic starts being generated early in the pulse, before significant ionization takes place, and therefore at an unshifted wavelength. It is also generated later in the pulse, when the intensity reaches the saturation intensity and therefore at a blueshifted wavelength. This leads to a rather large and regular broadening of the spectral profile, which, if we forget about the spatial effects, could be interpretated as a frequency chirp of the harmonic beam. This cannot occur in the 15th harmonic in xenon, because the plateau regime is not reached before saturation (Fig. 9). In that case, harmonic generation takes place predominantly at saturation intensity and the harmonic is much more uniformly shifted.

We have performed additional measurements for other (low-order) harmonics, in different conditions of pressure and intensity. Our conclusion is that these results confirm that the harmonics are spectrally shifted when the gaseous medium gets ionized. The spectral shift simply follows that of the fundamental. This effect begins just below the saturation intensity for the rare gases studied (10^{14} W/cm^2 in xenon and 2.5×10^{14} W/cm^2 in argon).

VI. SUMMARY

Using a high-repetition rate, short-pulse Ti-sapphire laser system, we have performed systematic studies of high harmonic generation in noble gases. By investigating the intensity dependences of the yields of the different harmonics, insight has been obtained regarding the formation of the characteristic plateau and the extent of this plateau as a function of the laser intensity.

At low intensity, the harmonics are in the cutoff region and their strength vary rapidly with the laser intensity. As the intensity increases, the harmonics join the plateau one after the other. The rate of variation with intensity of a given harmonic changes suddenly from the cutoff region (rapid variation) to the plateau region (slow variation, similar for all of the harmonics). Finally, the saturation intensity for ionization is reached and the yields of all harmonics saturate. For the high harmonics, the cutoff energy, i.e., the photon energy of the highest harmonic in the plateau, is found to increase linearly with laser intensity. The constant of proportionality, however, is smaller than that that predicted in the single-atom response. This effect is probably due to propagation effects in the tight focusing regime, which applies for the high harmonics.

In xenon and argon exposed to laser intensities much above the saturation intensities for ionization, we have observed harmonics well above the theoretical cutoff for the single-atom emission. The highest harmonics in these spectra, up to the 45th in Xe and 65th in Ar, are probably due to the contribution of ions. This is evidence for harmonic emission from ions using a low-frequency laser. It opens ways for reaching very short-wavelength coherent radiation [13].

Ionization of the nonlinear medium leads to time-dependent changes in the refractive index. This causes a spectral broadening and a blueshift of the laser radiation propagating through the medium. The spectral broadenings and shifts of the harmonics generated in the ionizing medium are found to be proportional to the broadening and shift of the fundamental laser radiation. Complex spatial and temporal effects may be suspected, which would deserve a detailed theoretical investigation.

ACKNOWLEDGMENTS

We are grateful to M. Lewenstein, K. C. Kulander, and K. J. Schafer for numerous discussions concerning these experimental results, to T. Auguste for his help concerning ADK tunnel ionization rates, to D. Cubaynes, J.- M. Bizeau, and P. Morin for their help in the calibration of our spectrometer at LURE, and to M. Bougeard, E. Caprin, and A. Sanchez for their skilled technical assistance. Financial support from the Swedish National Science Research Council, the Swedish Council for Planning of Research, and the Wallenberg Foundation is gratefully acknowledged.

[1] A. L'Huillier and Ph. Balcou, Phys. Rev. Lett. **70**, 774, (1993).
[2] J. J. Macklin, J. D. Kmetec, and C. L. Gordon III, Phys. Rev. Lett. **70**, 766 (1993).
[3] N. Sarukura, K. Hata, T. Adachi, R. Nodomi, M. Watanabe, and S. Watanabe, Phys. Rev. A **43**, 1669 (1991).
[4] K. Kondo, N. Sarukura, K. Sajiki, and S. Watanabe, Phys. Rev. A **47**, R2480 (1993).
[5] Y. Akiyama, K. Midorikawa, Y. Matsunawa, Y. Nagata, M. Obara, H. Tashiro, and K. Toyoda, Phys. Rev. Lett. **69**, 2176 (1992).
[6] K. Miyazaki and H. Sakai, J. Phys. B **25**, L83 (1992).
[7] Ph. Balcou, A. S. L. Gomes, C. Cornaggia, L. A. Lompré, and A. L'Huillier, J. Phys. B **25**, 4467 (1992).
[8] J. K. Crane, M. D. Perry, S. Herman, and R. W. Falcone, Opt. Lett. **17**, 1256 (1992).
[9] M. E. Faldon, M. H. R. Hutchinson, J. P. Marangos, J. E. Muffett, R. A. Smith, J. W. G. Tisch, and C. G. Wahlström, J. Opt. Soc. Am B **9**, 2094 (1992).
[10] J. W. G. Tisch, R. A. Smith, M. Ciarrocca, J. P. Marangos, and M. H. R. Hutchinson (unpublished).
[11] J. D. Kmetec, J. J. Macklin, and J. F. Young, Opt. Lett. **16**, 1001 (1991).
[12] K. Miyazaki (private communication).
[13] J. L. Krause, K. J. Schafer, and K. C. Kulander, Phys. Rev. Lett. **68**, 3535 (1992).
[14] W. Becker, S. Long, and J. K. McIver, Phys. Rev. A **41**, 4112 (1990).
[15] K. J. Schafer, K. C. Kulander, and J. L. Krause (private communication).
[16] P. B. Corkum, Phys. Rev. Lett. **71**, 1994 (1993).
[17] L. V. Keldysh, Zh. Eksp. Teor. Fiz. **47**, 1945 (1964) [Sov. Phys.—JETP **20**, 1307 (1965)]; F. Faisal, J. Phys. B **6**, L312 (1973); H. R. Reiss, Phys. Rev. A **22**, 1786 (1980).
[18] M. V. Ammosov, N. B. Delone, and V. P. Kraïnov, Zh. Eksp. Teor. Fiz. **91**, 2008 (1986) [Sov. Phys. – JETP **64**, 1191 (1986)].
[19] A. L'Huillier, M. Lewenstein, P. Salières, Ph. Balcou, M. Ivanov, J. Larsson, and C.-G. Wahlström, Phys. Rev. A **48**, R3433 (1993).
[20] A. L'Huillier, K. J. Schafer, and K. C. Kulander, J. Phys. B **24**, 3315 (1991).
[21] A. L'Huillier, Ph. Balcou, S. Candel, K. J. Schafer, and K. C. Kulander, Phys. Rev. A **46**, 2778 (1992).
[22] X. F. Li, A. L'Huillier, M. Ferray, L. A. Lompré, G. Mainfray, and C. Manus, Phys. Rev. A **39**, 5751 (1989).
[23] T. Auguste, P. Monot, L. A. Lompré, G. Mainfray, and C. Manus, J. Phys. B **25**, 4181 (1992).
[24] J. W. Cooper, Phys. Rev. **128**, 681 (1962)
[25] G.V. Marr and J.B. West, At. Data Nucl. Data Tables **18**, 497 (1976).
[26] J. J. Macklin (private communication).
[27] J. L. Krause, K. J. Schafer, and K. C. Kulander, Phys. Rev. A **45**, 4998 (1992).
[28] H. Xu, X. Tang, and P. Lambropoulos, Phys. Rev. A **46**, R2225 (1992).
[29] M. C. Downer, W. M. Wood, and J. L. Trisnadi, Phys. Rev. Lett. **65**, 2832 (1990).
[30] S. C. Rae and K. H. Burnett, Phys. Rev. A **46**, 1084 (1992).
[31] T. Auguste, P. Monot, L. A. Lompré, G. Mainfray, and C. Manus, Opt. Commun. **89**, 145 (1992).
[32] S. C. Rae and K. H. Burnett, J. Phys. B **26**, 1509 (1993).
[33] S. C. Rae and K. H. Burnett (unpublished).